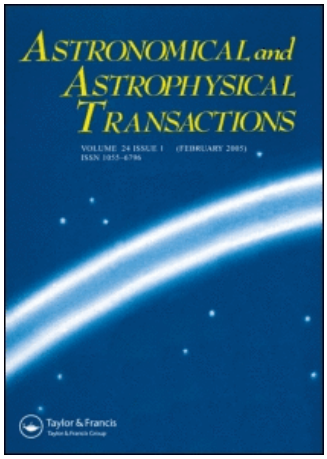

Astronomical & Astrophysical Transactions
The Journal of the Eurasian Astronomical Society
Publication details, including instructions for authors and subscription information:
http://www.informaworld.com/smpp/title~content=t713453505

THE β-PICTORIS PHENOMENON NEAR THE SUN

L. I. Shestakova [a]
[a] Fessenkov Astrophysical Institute, 480020 Almaty, Kazakhstan.

Online Publication Date: 01 April 2003
To cite this Article: Shestakova, L. I. (2003) 'THE β-PICTORIS PHENOMENON NEAR THE SUN', Astronomical & Astrophysical Transactions, 22:2, 191 - 211
To link to this article: DOI: 10.1080/1055679031000080339
URL: http://dx.doi.org/10.1080/1055679031000080339

Astronomical and Astrophysical Transactions,
2003, Vol. 22(2), pp. 191–211

THE β-PICTORIS PHENOMENON NEAR THE SUN

L. I. SHESTAKOVA[†]

Fessenkov Astrophysical Institute, 480020 Almaty, Kazakhstan

(Received May 29, 2002)

The results of the following investigations on dust and gas in the F corona are reviewed: firstly, interferometric observations of the radial velocities of dust using the Doppler shifts of Frauhofer lines obtained during two total solar eclipses on July 31, 1981 and July 11, 1991; secondly, modelling of the orbital evolution of dust grains near the Sun during their evaporation; thirdly, prediction of the resonance emission of gas formed near the Sun after evaporation of dust, solids and comets, together with the search for and discovery of emission in K line of Ca I, analysis of the Ca-ion acceleration mechanism, and a model of the expanding envelope; fourthly, the mechanism of thermal disintegration of both icy and non-icy bodies approaching the Sun in highly eccentric orbits, which was considered to be the source of dust grains and gas particles in the circumsolar region. Analytical and numerical solutions of the heat diffusion equation were used. Thermal stresses which arise inside and at the surface of solids can exceed by several orders of magnitude the tidal stresses in the neighbourhood of the Sun and play an important and possibly crucial role in the evolution of comet-like bodies.

Keywords: F corona, dust grains, solar eclipse, radial velocities, interplanetary dust, resonance emission, light pressure, meteoroids, comets, thermal stress, thermal disintegration, comet splitting

1 INTRODUCTION

It is difficult to represent the fact that near the Sun there can be processes showing active interaction with the surrounding matter. Reputedly, the phenomena associated with this activity, which are observed now only near young stars surrounded by a protoplanetary cloud, in the Solar System finished a long time ago. However, it is quite possible that many of these phenomena still occur today, but on a much smaller scale. Taking into account that the processes occurring near stars cannot be investigated in detail because of the major distances of these objects, circumsolar matter could become a good test object for investigation of similar phenomena.

Gurtovenko (1971) gave the first evidence of a comet falling on to the Sun. On July 28, 1966, he observed a strong sodium emission in an undisturbed region of the photosphere. However, this event, although unique, has remained almost unnoticed by scientists.

When there was a similar occurrence near the stars, the situation changed. So, after detection near β-Pictoris of the dust disc (Aumann *et al.*, 1984; Smith and Terrile, 1984), observations of this star in the resonance absorption lines of metals have begun: Na I, Ca II, Al III and others (Beust *et al.*, 1989; Vidal-Madjar *et al.*, 1994; Lagrange-Henri *et al.*, 1996). The

[†]Correspondence: L. I. Shestakova, Fessenkov Astrophysical Institute, 480020 Almaty, Kazakhstan.
E-mail: shest@afi.south-capital.kz

ISSN 1055-6796 print; ISSN 1476-3540 online
DOI: 10.1080/1055679031000080339

observations showed the presence of moving details inside the lines. This means that clouds of gas exist near the star. They are orbiting with high velocities exceeding Keplerian velocities. It appears that these observations are explained by comets falling on to a star and by their disintegration (Beust *et al.*, 1990; Beust and Morbidelli, 1996). Similar occurrences have also been found near other young stars (Grinin *et al.*, 1996).

Our predictions of the opportunity of observation of resonance emission of metals and their ions in a low-ionization state in the Na I, Ca I, Ca II, Mg I and Mg II near the Sun (Shestakova, 1990) have shown that the observations of gas emission formed after the evaporation of dust, meteoroids and destroyed comets are also quite real. For the first time, successful observations of the emission of a K line K of Ca II were carried out by Gulyaev and Shcheglov (199a,b) during the total eclipse of February 26, 1998. The observed velocities achieved values of about $280\,\mathrm{km\,s^{-1}}$. Also in the case of β-Pictoris, the acceleration of ions up to high velocities is mainly caused by radiation pressure of a central star (or the Sun) in the wavelengths of the respective resonance lines.

How can short-lived atoms and ions appear near the Sun? Evidently the source of these atoms could be dust, meteoroids and comet debris, which are able to approach the Sun. The cold gas observed near the Sun is formed during the evaporation of these solids.

The problem of cometary splitting has attracted considerable attention for many years. It has been discussed in the literature from different viewpoints by Sekanina (1982), Clube and Napier (1987), La Violette (1987), Dobrovolskis (1990), Benz and Asphaug (1994), Chen and Jewitt (1994), Pittish and Rickmann (1994), Bailey (1996), Steel (1996) and others.

New information about cometary splitting that occurred since the publication of the review by Sekanina (1982) led to the classification of split comets into two distinct groups depending on the break-up products (Sekanina, 1997): non-tidally split comets which should have fragments considerably less massive than the principal nucleus, and tidally split comets which should have fragments of comparable masses. The statistics showed that by 1996 there were 28 known non-tidally and five tidally split comets (Sekanina, 1997).

The break-up mechanism leading to non-tidal splitting is not known definitely at present. Some causes such as stresses due to rapid rotation, temperature gradients and the presence of volatiles have been considered in the literature; in the paper by Shestakova and Tambovtseva (1997–1998) the present authors and a co-worker gave a brief review of these mechanisms.

Experiments connected with the investigation of radial velocities of dust in the F corona were our first topic of research in this field. Interferometric observations of the radial velocity field in the F corona during the total solar eclipse on July 31, 1981 (Shcheglov *et al.*, 1987; Shestakova, 1987), permitted us to obtain a two-dimensional distribution of the dust radial velocity in the elongation range from $3r_\odot$ to $7r_\odot$ where $r_\odot$ is the solar radius. The Fraunhofer lines in the spectral region of Mg I ($\lambda = 5184$ Å) were used. To analyse the results obtained near the ecliptic plane we suggested an undisturbed distribution of the dust grain concentration depending on the heliocentric distance according to the law $n(r) = n_0 r^{-\nu}$ for $r > r_0$ where r_0 is a radius of the dust-free zone (DFZ) near the Sun.

Calculations showed that the model parameters $\nu = 1.1$ and $r_0 = 6.5r_\odot$ and the mean dust grain radius $\bar{s} = 0.4\,\mu\mathrm{m}$ satisfied these observations. Observed projections of the velocities on the line of sight coincide with the Keplerian dust motion at a distance near $15r_\odot$. We showed that beyond this distance no new increase in the concentration n_0 can exist in addition to the undisturbed power law. Regions of enhanced dust concentration can exist in the distance range from $6.5r_\odot$ to $15r_\odot$.

During the total solar eclipse on July 11, 1991, we tried to repeat this experiment (Aimanov *et al.*, 1995). Observations of radial velocities in the F corona in the elongation range from $3r_\odot$ to $7r_\odot$ were carried out (La Paz, Mexico) by means of a Fabry–Pérot spectro-

graph. The Fraunhofer lines in the spectral region of the H and K lines of Ca II were used. The average velocities to the west and to the east of the Sun within 30° of the ecliptic plane were found to be $+30\,\mathrm{km\,s^{-1}}$ and $-27\,\mathrm{km\,s^{-1}}$ respectively. This confirmed the main results of the F-corona radial velocity observations made by Shcheglov *et al.* (1987) and Shestakova (1987) on July 31, 1981 about the predominance of prograde Keplerian motion of dust near the ecliptic plane and the effective radius of the dust grains (about 0.4 μm).

Dust behaviour investigations in the F corona were continued by means of computer modelling of the orbital evolution of dust grains. The orbital motion of interplanetary dust grains in the sublimation zone near the Sun has been considered for graphite and silicate grain material. Calculations showed that dust grains with initial radii $s = 0.5$–$5\,\mu\mathrm{m}$ can form regions of enhanced concentration. The inner corona is slightly enriched with particles of radii $s = 0.3$–$0.6\,\mu\mathrm{m}$ because the evaporated grains move into highly elliptic orbits. However, they may be not recognized owing to their small contribution to the total brightness along the line of sight compared with the background of the more typical zodiacal particles with $s \approx 30\,\mu\mathrm{m}$. An enhanced number density of small grains may be visible slightly beyond the ecliptic plane (Shcheglov *et al.*, 1987).

Thus a simple scenario of the circulation of matter in the Solar System is looked at; comets falling on to the Sun or Sun-grazing comets became a source of many small fragment and dust grains. The evaporating solids first result in the small dust particles in the F corona, and form clouds of cold gas. Further, some atoms and ions having strong resonance lines in the region, where the solar continuum spectrum is intensive, can appear under the action of strong radiation pressure and be accelerated, leaving the Sun with various velocities. For such atoms and ions the Sun acts as a separator, creating clouds consisting of atoms or ions of one type. Clouds leave the Solar System, where they are mixed as a final result with solar wind particles return again to the interstellar medium, supplementing the material for the formation of new generation of stars, planets and comets.

Next we discuss in more detail the problems connected with observations of radial velocities of dust in the F corona, numerical modelling of the orbital evolution of evaporating dust particles, the search for resonance emission of gas and the problem of the thermal disintegration of comets, a mechanism that influences of comets and is the evolution probably a little underestimated today.

2 THE RADIAL VELOCITY FIELD OBSERVATIONS

The observational method was described by Aimanov *et al.* (1995). The centre of the interference rings coincide with that of the Sun's image. The Doppler shifts were measured relative to identical Fraunhofer features of the spectrum, of the day time sky obtained just after the total phase. We used several radial scans with the position angles shown in Figure 1. The Doppler shifts were obtained along each measured scan at the points of intersections with Fraunhofer rings. The results averaged with two, the methods are presented in Figures 1 and 2. Figure 1 shows the dependence of the mean radial velocity on the position angle. It is seen that velocities are negative in the east and positive in the west. This confirms the existence of dust moving on Keplerian orbits in the prograde direction. Figure 2 shows the mean dependence of the radial velocities on elongations. Points are obtained by averaging in the range of 30° near the ecliptic plane. The east, west and mean (east–west) directions are given separately.

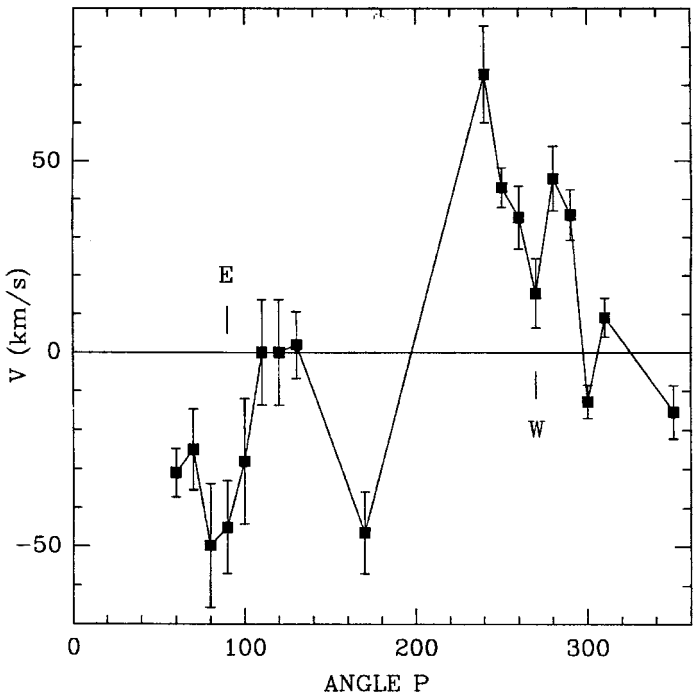

FIGURE 1 The dependence of the observed radial velocity on the position angle. The points are obtained by averaging over elongations in the range (3–5)$r_{\odot}$. The beginning of the observation, 0°, is in the direction of the north pole of the ecliptic plane.

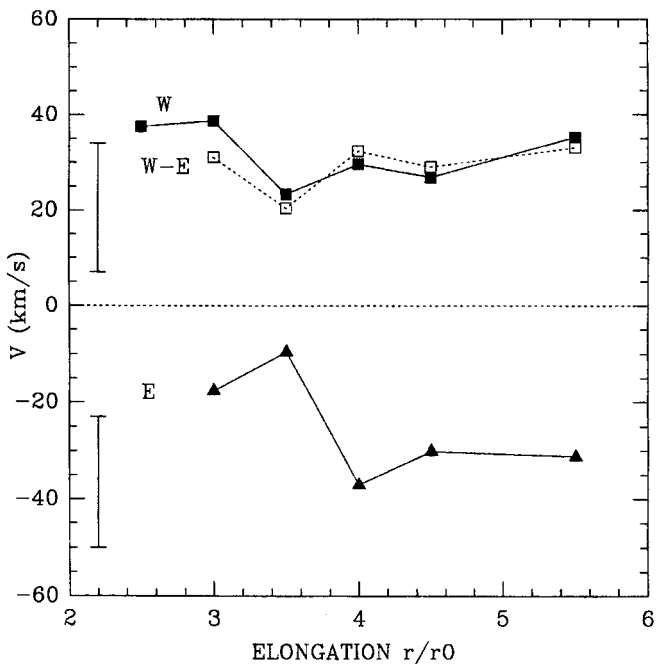

FIGURE 2 The mean radial velocities near the ecliptic plane (±30°) as a function of the elongation. The range of averaging over the elongation is 0.5$r_{\odot}$.

According to Shestakova (1987), observations of the velocity in the F corona are presented as the average valve weighted over the brightness in the form of an integral along the line of sight:

$$V(\epsilon) = \frac{\mu V_{\mathrm{E}}}{\sin^{1/2}\epsilon} \frac{\int_{\epsilon}^{\pi} \sin^{\nu+3/2}\theta\, \sigma(\theta)\, \mathrm{d}\theta}{\int_{\epsilon}^{\pi} \sin^{\nu}\theta\, \sigma(\theta)\, \mathrm{d}\theta}, \tag{1}$$

where

$$\sigma(\theta) = s^2\left(\frac{A}{4} + \frac{J_1^2(\kappa \sin\theta)}{\sin^2\theta}\right)$$

is a function of diffraction scattering, ϵ and θ are the elongation and scattering angle respectively, V_{E} is the orbital velocity of the Earth, $\mu = (1-\beta)^{1/2}$ is a coefficient taking into account the effect of radiation pressure, β is the ratio of radiation pressure to gravity, s is the grain radius, A is the albedo, $\kappa = 2\pi s/\lambda$ is the size parameter and J_1 is a Bessel function. Since observations were made through the DFZ each integral in equation (1) is divided into two parts with the following limits: the first from ϵ to θ_0, and the second from $\pi-\theta_0$ to π, where $\theta_0 = \arcsin[(R_0 \sin\epsilon)/r_0]$ and $R_0 = 1$ AU.

When $\nu = 1$, an analytical solution of equation (1) is possible in the elongation range $R_0\epsilon < 0.7 r_0$:

$$V(\epsilon) = \frac{4\mu V_{\mathrm{E}}(R_0/r_0)^{1/2}}{\pi\bar{\kappa}}, \tag{2}$$

where $\bar{\kappa}$ is a mean effective size parameter. Using equation (2) means fulfilment of two conditions $\bar{\kappa}\theta_0 \gg 1$ (large grains) and $\bar{\kappa}\epsilon \ll 1$ (small angles). In fact for observations in the solar corona in the optical region this restriction means that equation (2) can be used when $0.2\ \mu\mathrm{s} < \bar{s} < 3\ \mu\mathrm{m}$. If one considers in equation (1) a more realistic scattering function, weighted over a grain size distribution in the form $n(s) = n_0 s^{-p}$, then the analytical solution of equation (1) can also be obtained in some cases. For example, in the case when $p = 4$, we obtain an expression such as equation (2) with $2\kappa_1$ instead of $\bar{\kappa}$, κ_1 is the lower limit of this parameter corresponding to the lower limit of the grain size s_1. From equation (2) it follows that $\bar{s} \approx 0.5\ \mu\mathrm{m}$ (or $s_1 \approx 0.2\ \mu\mathrm{m}$), close to the results of our numerical calculations. In Figure 3 we present results of numerical calculations of the radial velocity (equation (1)) with $\nu = 1.1$, $\bar{s} = 0.45\ \mu\mathrm{m}$ and $r_0 = 7 r_{\odot}$, giving good agreement with both observations. For comparison we give the observational results obtained in 1981 (Shestakova, 1987) and in 1991 (Aimanov *et al.*, 1995). Equation (2) corresponds to the inner flat part of the curve in Figure 3.

In order to compare the results of the different methods to observe the F corona it is necessary to consider a weighting function looking like $\sin^{\alpha}\theta$ in the corresponding integrals. We have $\sin^{\nu+3/;2}\theta$ for the method of radial velocities, $\sin^{\nu}\theta$ for the brightness integral and $\sin^{\nu-2}\theta$ in the expression for the thermal emission integral. It can be seen that $\sin^{\nu+3/2}\theta$ is most appropriate for the contribution of the coronal region where $\theta \approx 90^{\circ}$; thus, the dependence of the results on the choice of the model is minimal. Moreover, there exists direct evidence that the results refer to the region of the F corona: firstly, the projections of the circular velocities on the line of sight for the particles beyond $17 r_{\odot}$ are less than those that we measured during the two eclipses; secondly, the more precise and complete data on radial velocities in the corona in 1981 definitely indicate an increase in the observed velocity with increasing elongation. This is possible if we make observations through the DFZ; beyond this zone the Keplerian law V is proportional to $1/r^{1/2}$ has to be obeyed (Figure 3).

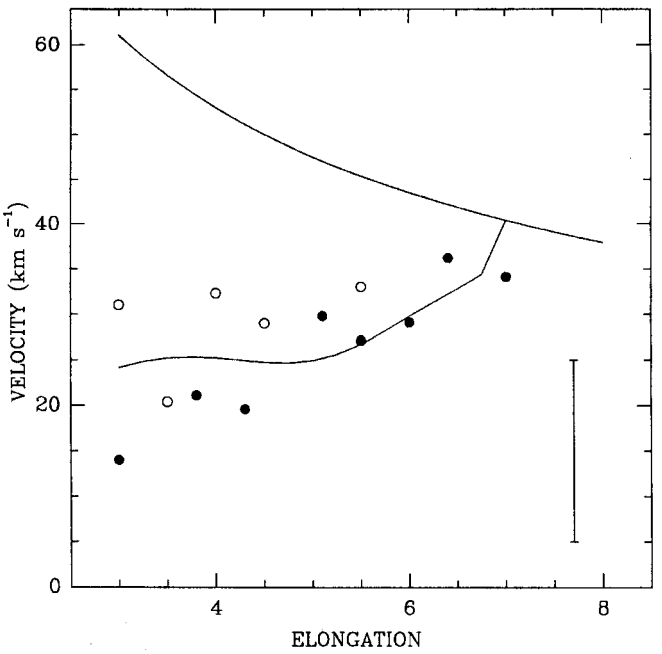

FIGURE 3 The calculated radial velocities versus elongation in solar radii. The parameters are $v = 1.1$, the grain radius $s = 0.45$ μm and $A = 0.25$. The upper solid curve is the case when a DFZ is absent, and the lower solid curve is when the radius of the DFZ equals $7r_{\odot}$. The full circles are the observations made in 1981, and the open circles are those made in 1991.

Using the suggestion of an undisturbed distribution of the dust concentration according to the law $n(r)$ is proportional to r^{-v} in the observed range of distances $6.5r_{\odot} < r < 17r_{\odot}$, we found that the main contribution to scattering is made by the grains with $s = 0.4$–0.5 μm, that is, one to two orders of magnitude less than those of the zodiacal cloud. The size may be changed if an excess of concentration is detected in the distance range mentioned above.

The existence of such a large DFZ for the usual zodiacal dust does not exclude the penetration of large comet-like bodies, whose remnants can reach $(4.0$–$4.3)r_{\odot}$. The second possible way to increase the contribution of the corona to the brightness along the line of sight is to change the scattering function $\sigma(\theta, \kappa)$. When observing in the near-infrared region, the parameter κ decreases because λ increases. This is equivalent to increasing the contribution of smaller grains in the volume scuttering function (VSF). The infrared observations of the F corona in 1991 (Lamy *et al.*, 1992; Mann and MacQueen, 1993) showed that for small elongations the observed intensity was significantly higher than calculated using the VSF of the visible region. We favour the model with undisturbed dust distribution up to the DFZ as more reliable because of the absence of thermal emission in the corona in 1991 (Hodapp *et al.*, 1992; Lamy *et al.*, 1992). An excess of small dust grains in the F corona, invisible in observations of the brightness but seen with the radial velocity method, is confirmed by our calculations (Shestakova and Tambovtseva, 1995).

3 ORBITAL EVOLUTION OF DUST GRAINS

Calculations of the dynamics of the dust particles such as silicate and graphite (Lamy, 1974; Mukai and Yamamoto, 1979) made after detecting the thermal emission excess in the F

corona in the near-infrared region of the spectrum at $\lambda = 2.2$ and 3.5 μm (Peterson, 1967; MacQueen, 1968) showed that during the evaporation process the orbital evolution of the dust grains, represented as a dependence of the heliocentric distance on the revolution number, often demonstrates a 'turnaround'. This means that the falling of the grains on to the Sun under the Poynting–Robertson (PR) effect stops and during some time the return motion (from the Sun) could occur. It appeared that, near 'turnaround', one could expect an enhancement in the grain concentration.

The model suggested by Mukai and Yamamoto (1979) predicts an increase in the graphite grain concentration by a factor of 10 in the range of distances (4.0–4.3)$r_\odot$ and an increase in the silicate grain concentration by a factor of 5 in the range (4.0–4.6)$r_\odot$. However, new observations of the thermal emission in the F corona in 1991 (see for example Hodapp *et al.* (1992) and Lamy *et al.* (1992)) did not reveal any special features until distances of $15r_\odot$. According to Mann and MacQueen (1993) the brightness distribution in the F corona at $\lambda = 2.12$ μm is explained by strong thermal emission of the dust with a power-law dust distribution typical for the zodiacal cloud without an excess concentration.

We carried out dynamic calculations for p- and r-obsidian (with poor and rich contents of FeO respectively), basalt, astronomical silicate (ASIL) and graphite. The method has been described in detail by Shestakova and Tambovtseva (1995). Our goal is to check the validity of the models predicting enhancement in the concentration for grains with sizes typical for particles of zodiacal light in the narrow ring-like zones of the F corona.

The thermal balance was computed using data on refractive indices for the grains of interest and the new data on the solar radiation flux in the wavelength range 0.15–50 μm; the energy contribution beyond this range is negligible (see Shestakova and Tambovtseva (1995) and references therein). The temperature distribution of the silicate grains, the sublimation rate of which is computed according to Lamy (1974), reflects the order of location of the sublimation zones for different types of silicate (Figure 4). The calculations show that the temperature of the silicate grains near the 'turnaround' point lies in the range 1300–1200 K while for graphite grains the same sublimation rate is reached at 2000–1900 K. Particles consisting of mixed materials (see for example Mann *et al.* (1994)) are not

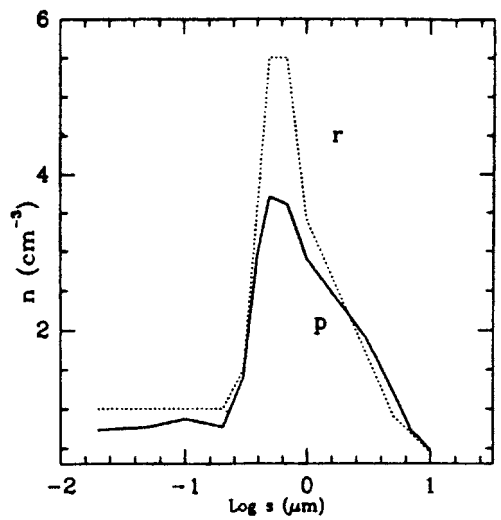

FIGURE 4 The ratio of the number density in the narrow region with the width $0.5r_\odot$ to the normal number density for p- and r-obsidian as a function of the initial grain size. The lower boundary of the region coincides with τ_{min}, the 'turnaround' point of the grain orbital evolution ($2.6r_\odot$ and $4.7r_\odot$ for p- and r-obsidian respectively).

considered here but it should be noted that differences in the sublimation rates could change the chemical composition and other features of the dust approaching the Sun.

Calculations of the orbital evolutions show that all grains considered with initial sizes $s_0 > 0.5\,\mu m$ make the 'turnaround' and after passing a certain distance r_{min} the ellipticity of their orbits increases. This increase is due to the rapid increase in the radiation pressure when the radii of the silicate grains reach $s_{max} = 0.2$–$0.25\,\mu m$, corresponding to the maximal ratio of the radiative force to the gravitational force β_{max}.

We computed the ratio of the grain lifetime τ in the narrow region (width, $0.2r_\odot$), which has a lower boundary coinciding with r_{min} of the orbital evolution, to the time t_{PR} of the grain's drift through this region under the effect of PR drag in conditions when the grain size does not change. This ratio τ/t_{PR} reflects the change in number density n of the grains of given composition and initial sizes in the region compared with the normal valve n_u corresponding to the undisturbed state. It is seen from Figure 4 that any noticeable increase in n for p- and r-obsidian grains (by a factor of 2 and more) is possible only in the initial size range $s_0 = 0.4$–$3.0\,\mu m$ with the maximum near $s_0 = 0.5$–$0.7\,\mu m$.

The possible concentration of dust grains in the narrow region is connected with the value of r_{min} practically, that is with the position of the boundary of the DFZ for grains of a given composition. If for grains of different sizes the points r_{min} of the 'turnaround' are spatially separated, then one should not expect a real enhancement in the concentration, even for the limited range of grain sizes mentioned above. Thus it is possible that p- and r-obsidian grains are concentrated in the narrow region since the value of r_{min} for all grains (with $n > 1$) is constant. For grains of other materials this condition is not fulfilled. So, the width of the region of possible concentration of the basalt-like and graphite grains expands to $(0.5$–$1.0)r_\odot$ and for ASIL to $(5$–$10)r_\odot$. Thus, an enhancement in the concentration for ASIL-like particles in the narrow region is unlikely.

When basalt and obsidian grains reach their critical sizes s_{max}, their orbital evolution terminates with a steep fall towards the Sun; as graphite particles have evaporated to a size of $0.5\,\mu m$, they leave the Sun. The ASIL grains demonstrate a different behaviour; those with $s_0 < 0.2\,\mu m$ fall towards the Sun and evaporate at about $14r_\odot$; as those with $s_0 = 0.3$–$3\,\mu m$ have evaporated to a size of $0.3\,\mu m$, they leave the Solar System. The larger grains with $s_0 > 5\,\mu m$ after approaching r_{min} (near approximately $10r_\odot$) begin to move away from the Sun but evaporate completely at the same distances as the smaller grains.

The calculations show that dust grains of the micron sizes typical for zodiacal light with initial sizes $s_0 > 5\,\mu m$ cannot form the dust rings because of the dynamic evolution of their orbits in the sublimation zone near the Sun. The same conclusion refers to grains with $s_0 < 0.3\,\mu m$. The narrow ($(0.2$–$0.5)r_\odot$) dust rings of enhanced concentration can be formed by grains with initial radii $s_0 = 0.4$–$3.0\,\mu m$ consisting of weakly absorbing sorts of silicate (obsidian and basalt), and also by graphite particles with $s_0 = 0.5$–$5.0\,\mu m$. All of these evaporate at distances $r < 10r_\odot$. The maximal increase in concentration is possible by grains with radii 0.5–0.7 μm. It is worth noting that the radial velocity observed in the F corona in the elongation range $3r_\odot$–$7r_\odot$ indicates that in the circumsolar region along the line of sight, beyond the sharp internal boundary, the dust grains with $s = 0.4$–$0.5\,\mu m$ are predominant (Aimanov *et al.*, 1995).

After leaving the stationary orbit the graphite grains, evaporated to a size of $0.5\,\mu m$, and some ASIL grains, evaporated to a size of $0.3\,\mu m$, become β-meteoroids, leaving the Solar System. Dust grains with optical properties similar to ASIL sublimating far from the Sun go into elliptical orbits and reach the Earth. In this case near the aphelion of their orbits they can be observed as α-meteoroids or 'apex' particles with a small angular momentum and a mass of 10^{-12}–10^{-13} g. Such particles were observed in the inner Solar System during the Helios 1 and Helios 2 missions.

4 COLD GAS IN THE SOLAR CORONA

It is known that dust particles of the zodiacal cloud are spiralling slowly towards the Sun under the action of the PR effect. The dust particles evaporate at some distance from the Sun and transform into gas, the temperature of which is less by some orders of magnitude than the temperature of the environment gas of the corona.

Another way in which a cold substance can penetrate the circumsolar region is by comets of the Kreutz group falling on to the Sun or by Sun-grazing comets. Such comets can be completely destroyed and transform into gas during one passage through the perihelia of their orbits. The appearance of interplanetary matter in the solar corona was confirmed by the SOHO mission, which records many Sun-grazing comets every year.

What happens to the cold gas formed after evaporation of zodiacal and cometary dust in the environment of the solar corona?

According to calculations, carried out some years ago (Shestakova, 1990), the lifetime of atoms and most of the initial ions with low ionization potentials is limited by rate of their ionization by ultraviolet radiation from the Sun. When an atom losses two or three electrons, its further ionization is caused as a rule by collisions with particles from the corona, because owing to the high potentials of each subsequent stage of ionization the probability of radiative ionization becomes less.

It is possible to consider the process of transformation from a cold gas into a hot coronal gas to be completed after an ionization balance is approached, which in the conditions of solar corona occurs at high stages of ionization. It is not our aim to study this complex process of the transition of a cold gas into coronal gas, which can occur in the case of penetration of interplanetary matter inside a dense region of the corona. We only consider the dynamics of the initial Ca ions; their resonance luminescence was recently discovered by Gulyaev and Shcheglov (1999a,b) in the outer solar corona during the total solar eclipse on February 26, 1998, and confirmed by new observations on August 11, 1999 (Gulyaev and Shcheglov, 2001).

The first prediction of the possibility of detecting the emission of some atoms and low-ionization ions formed after sublimation of zodiacal dust was published by Shestakova (1990). Soon after, searches for the presence of a cold substance in the external solar corona began.

Some attempts to detect the resonance emission of Ca ions using Shcheglov's device were made during total solar eclipses. The sensitivity of the device was increased from one eclipse to another, and finally the success was achieved. The first attempt at interferometric observations was made on July 11, 1991 in Mexico, La Paz (by A. K. Aimanov, L. I. Shestakova and P. V. Shcheglov). It appeared that there were emission rings covering the total field of view, reaching about 30° on a photograph with the longest exposure. As was found after the analysis, the rings of emission belong to mercury ($\lambda = 3906.4$ Å).

Further interferometric observations on March 9, 1997 in the Chita region of Russia carried out by R. A. Gulyaev and P. V. Shcheglov showed that the instrument has a good sensitivity, as all the eclipsed sky was covered by rings of the H and K absorption lines of Ca II. However, no emission was found. Only during the eclipse of February 26, 1998 in Guadelupe the wide-field interferometric observations of the F corona in the H and K lines of Ca II (Gulyaev and Shcheglov, 1999a,b) have shown the presence of Ca II, emission in several parts of interferogram to the west of the Sun.

The intensity of the observed emission at the centre of an absorption line appeared to be equal approximately to the intensity of the continuous spectrum between the lines. According to Kout'chmy (1998) the brightness of the eclipsed sky at the place of observations was

2×10^{-9} times lower than the brightness of the solar disc centre. According to Allen (1963) the intensity of the continuum near $\lambda = 3900$ Å was approximately equal to 4.4×10^6 erg cm^{-2} s^{-1} sr^{-1} Å^{-1}. Thus the observed value of continuous spectrum intensity near the K line of Ca II is equal to about 8.8×10^{-3} erc cm^{-2} s^{-1} sr^{-1} Å^{-1} and, if the full width of half-maximum equals 1 Å, it agrees well with the estimations of the K-line intensity of Ca II carried out by Shestakova (1990). According to the above-cited paper, the estimation of intensity of the resonance emission of the K line of Ca II at a distance of $6r_\odot$ is the following: $1.6 \times (10^{-2}$–$10^{-3})$ erg cm^{-2} cm^{-2} s^{-1} sr^{-1}.

A model of the movement of Ca ions leaving the parent body allows us to estimate the conformity of a suggested mechanism of acceleration to observed velocities and to evaluate some orbital parameters of the initial parent body using also the configuration of observed emission.

The model of Ca-ion motion is constructed using the following assumptions.

(i) Ca atoms appear after the break-up of small bodies of Solar System, which move in Keplerian orbits with an eccentricity $e \leqslant 1$.

(ii) The influence of the corona, interactions and collisions with particles of the corona are neglected, as the relaxation time of a Ca ion of the first ionization stage with the corona (slowing-down time of Ca ions at protons) at a distance $6r_\odot$ according to theory (Alfvén and Feltkhammar, 1967) and after our estimations is approximately $t_s(i, p) = 2.1 \times 10^6$ s. This value is higher by an order of magnitude than the lifetime of the ion before its subsequent ionization by ultraviolet radiation of the Sun, which from the estimations by Shestakova (1990) is equal to 1.5×10^5 s. An estimation for $t_s(i, e) = 1.45 \times 10^7$ s (the slowing-down time of Ca ions at electrons) has a value that is an order of magnitude greater than the above-mentioned $t_s(i, p)$. Thus, consideration of any process of interaction between Ca ions and particles of the corona is useful only after their transition to the subsequent stage of ionization, but then the emission from the K line of Ca II has disappeared.

(iii) The motion of a neutral atom is excluded from view and we shall just calculate the motion of an ion after leaving the parent body, because at a distance of $6r_\odot$ from the centre of the Sun a Ca atom will be ionized within 160 s.

The force acting on an ion along the radius vector can be summarized as follows:

$$M\ddot{\boldsymbol{r}} = F_K + F_H + F_g + F_M, \tag{3}$$

where $\ddot{\boldsymbol{r}}$ is the radial acceleration, m is the mass of a Ca ion, F_K and F_H are the radiation pressures in the K and H resonance lines respectively of Ca II, F_g is the gravitational force and F_M is the force caused by action of a magnetic field, considered (in the first-order approach) to be averaged for one period of gyration.

In the radial field of the Sun the action of this force will appear as 'magnetic mirror acceleration' or gradient drift of the guiding centre of a particle to the region of the weaker field, that is away from the Sun. In this case, equation (3) will be the equation of movement of the guiding centre, around which cyclotron rotation of a particle occurs.

The numerical estimations have shown that the main reason for ion acceleration is the radiation pressure. The gravitational force and 'magnetic mirror acceleration' in the outer radial magnetic field at the moment of a separation from a parental body almost compensate for the Ca ion. For accounts of radiation pressure at a given Doppler shift the intensity of H- and K-line solar spectrum features of Ca II, according to Minnaert *et al.* (1940) is used. The level of the continuous spectrum near the lines is that according to Allen

(1963). After acceleration of ions up to Doppler shifts $\lambda > 5$ Å, the intensity of the H- and K-line solar spectrum of Ca II reaches 60% of the level of continuum and in this case the relation between the radiation pressure and the gravitational force is $\beta = (F_K + F_H)/F_g = 15.7$.

The observed emission details are like those of luminous arcs, that are fragments of interference rings. They are visible in those places where there is a luminous substance (Gulyaev and Shcheglov, 1999b). The geometry of emission shows (Figure 5) that almost all the emission region is to the west of the Sun. This start and the end of emission, following an imaginary orbit of a parental body moving from the south to the north around the Sun, symmetrically expands outwards the limits of the north–south axis to the east. Therefore we assume that the perihelion of the parent body orbits lie in a plane of an east–west ecliptic plane to the west of the Sun.

Using the configuration of emission in Figure 5 and the observed radial velocities (Gulyaev and Shcheglov, 1999b) it is possible to estimate the orbit parameter of the parent body, $p = 2q$, where q is the distance of the perihelion, and also the angles i and δ, where i is the angle of declination of the orbit to the ecliptic plane and δ is the angle of rotation of the orbit relative to the plane of the picture. Near the quadratures, where $\varphi = 90°$, the distance of the body from the Sun coincides with the orbit parameter, $r = p$; therefore, using the position of inner boundaries of emission (Figure 5), we can find that $p = (3.5\text{–}4.7)r_\odot$. Taking into account all the observed data, the current values of orbit parameters of the parent body are obtained: $p = 4r_\odot$, $i = 70°$, $\omega \approx 0°$ and $\delta = 11°$. It follows that the initial orbit of the body is close to the plane of the picture. Therefore, if the model in Figure 5 is accepted, $i = 90°$ and $\delta = 0°$.

The spacious region of gas emission simultaneously observed from $\varphi = -90°$ to $\varphi = +90°$ cannot be explained by the passage of one parent body. It needs a stream of vaporizing bodies. It is possible to estimate the length of the 'meteoric' stream in the orbit using the iso-

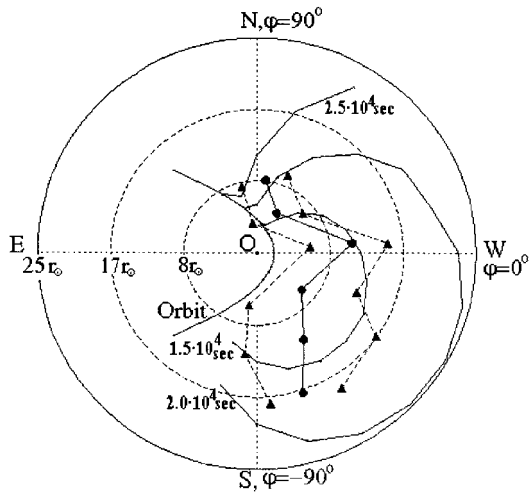

FIGURE 5 The geometry of the emission in a K line of Ca II, observed by Gulyaev and Shcheglov (1999b). Along the east–west line the radii of circles are indicated in terms of the solar radius $r_\odot$. The full circles show the centres of luminous arcs, and the full triangles their exterior and interior edges. The region of emission is limited inside by the orbit of the parent body. The perihelion $q = 2r_\odot$. The lines of isochrones computed according to the model are marked. The moment $t = 0$ for isochrones coincides with the position of quadrature on an orbit, where an orbit intercepts the line OS ($\varphi = 90°$).

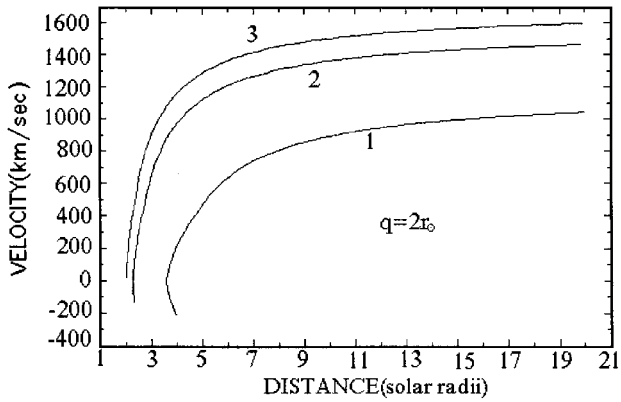

FIGURE 6 The velocity of ions versus the distance after starting from the parabolic orbit of the parent body, for which $q = 2r_{\odot}$. Three trajectories are given: curve 1, the ion starts in a quadrature, with $\varphi = -90^{\circ}$ and $r_{st} = 4r_{\odot}$; curve 2, the ion starts at an intermediate point of an orbit, with $\varphi = -45^{\circ}$ and $r_{st} = 2.34r_{\odot}$; curve 3, the ion starts in the perihelion with $\varphi = 0^{\circ}$ and $r_{st} = 2r_{\odot}$.

chrones of emission drawn in Figure 5. All the observed emission is located inside the 25^3 s isochrones. During this time the body passes more than 180° round a perihelion.

The radial velocities for the ions that survive and move away from the Sun are shown in Figure 6. The velocities obtained are very high in comparison with the observed velocity. After repeated successful observations carried out in Bulgaria during the total solar eclipse on August 11, 1999, Gulyaev and Shcheglov (2001) found three radial velocities of about $-420\,\mathrm{km\,s^{-1}}(19r_{\odot})$, $+490\,\mathrm{km\,s^{-1}}(21r_{\odot})$ and $-830\,\mathrm{km\,s^{-1}}(24r_{\odot})$. Thus, in the vicinity of the Sun the motion of Ca II ions with radial velocities of different signs and values close to $1000\,\mathrm{km\,s^{-1}}$ can be observed.

The estimation of the total mass of emitted Ca ions is approximately 1.5×10^9 g with a columnar concentration of about $1.9 \times 10^6\,\mathrm{atoms\,cm^{-2}}$. For a porous body of cometary type with an ordinal abundance for the Solar System according to Allen (1963), the estimation of mass will be about $M_{com} = 2.6 \times 10^{13}$ g, that is equivalent to a body of radius 0.22 km at a mass density equal to $0.6\,\mathrm{g\,cm^{-3}}$.

Our investigations of the processes of transition of dust and small bodies into gas in the circumsolar region, similar to those near β-Pictoris, are unique and further development is required.

5 THE THERMAL DESTRUCTION OF SOLIDS NEAR THE SUN

Here we study a possible mechanism that can cause disintegration of icy and non-icy bodies moving in parabolic orbits. This mechanism was considered by Kürt (1984) who computed the temperature profiles for several heliocentric distances of Halley's comet, solving numerically the heat diffusion equation (HDE) in order to estimate the thermal stresses. According to Kürt a 3 km spherical icy body moving in the orbit of Halley's comet undergoes, at perihelion, thermal stresses in its centre that are lower than the tensile strength by only one order of magnitude. At the same time, the thermal stresses at the surface, down to a depth of 10 m, exceed the strength of the material by a factor of more than 10. Thus, he concluded that the thermal stresses may lead to the formation of cracks in comet nuclei. Later Tauber and Kürt (1987) calculated the thermal stresses due to the temperature gradient between the surface and the core for more realistic cometary nuclei composed of weakly attached cometesimals and showed that they can evoke cometary splitting or outbursts.

Shestakova and Tambovtseva (1997–1998) investigated the problem of disintegration of both icy and non-icy bodies in the Solar System. The temperature distribution between the surface and the inner part of the solids has been calculated by means of the analytical solution of the time-dependent HDE in order to derive thermal stresses inside the bodies approaching the Sun in parabolic orbits. It was shown that the thermal destruction can play a crucial role in the splitting of solids. We mentioned that in order to distribute the fragments along the orbit, forces other than the thermal stresses are needed. Such mechanisms as tidal forces, rapid rotation and the presence of volatiles in the solids may overcome self-gravity and spread the fragments along the orbit.

An analytical analysis of the non-icy solids gives quite reasonable results (Shestakova and Tambovtseva, 1997–1998). To obtain more accurate temperature profiles and thermal stresses arising in the interior and on the surface of an icy solid, we addressed this problem by solving numerically the nonlinear time-dependent HDE (Tambovtseva and Shestakova, 1999). The results of analytical solution and numerical calculations almost coincide.

5.1 Solution of the heat diffusion equation

The HDE for a spherical body has the form

$$c_v \frac{\partial T}{\partial t} = \frac{\partial}{\partial x}\left(\kappa(T)\frac{\partial T}{\partial x}\right) + \frac{2}{x}\kappa(T)\frac{\partial T}{\partial x}, \tag{4}$$

where x is the current coordinate along the radius r of the body. The specific heat $c_v(T)$ per unit volume and the thermal conductivity $\kappa(T)$ in common cases are functions of the temperature. This equation can be solved together with one initial condition and two boundary conditions for the centre of the body at $x = 0$ and for its surface at $x = r$. The boundary condition for the centre of the spherical body is universal and follows from the symmetry of the body; $\mathrm{d}T/\mathrm{d}x|_{x=0} = 0$.

The initial condition and the surface boundary conditions have to be chosen in view of the actual physical conditions. At the initial moment the body's volume is assumed to be isothermal at some initial distance R_0; in other words, we put $T(x) = T_s$, where T_s is the equilibrium surface temperature. For the icy solids, $R_0 \geqslant 100$ AU (Oort cloud) or 30 AU (Kuiper belt). The solids of other materials start from 1 AU. The solids do not retain the initial temperature in their centres when approaching the Sun and, therefore, a choice of initial distance for them is not necessary.

The main problem is to find the surface boundary condition. This condition follows from the thermal balance, and for massive solids it has the form (Kürt, 1984)

$$\frac{(1-A)r_\odot^2\sigma T_{\mathrm{eff}}^4}{4R^2} = \varepsilon\sigma T_s^4 + \kappa(T_s)\left.\frac{\mathrm{d}T}{\mathrm{d}x}\right|_{x=r} + LZ(T_s), \tag{5}$$

where $r_\odot$ and T_{eff} are the radius and the effective temperature respectively of the Sun, R is the distance from the Sun, σ is the Stefan–Boltzmann constant, ε is the emissivity, A is the albedo, L is the latent heat of sublimation and Z is the sublimation flux.

Here it is supposed that the solar energy gain is restricted to one hemisphere, that the solid body rotates and that the surface is isothermal and radiates isotropically. To find an analytical solution of the HDE we introduce some simplifications both for equation (4) itself and for thermal balance equation (5) at the surface of the solid body.

(i) The thermal parameters c_v and κ do not depend on T; that is, we solve the linear HDE. Such a supposition is quite satisfactory for silicate and iron and also, at a stretch, for graphite (at high temperatures) (Campbell, 1956). For ice the dependence of these coefficients on T is more marked and the solution of the HDE given below is approximative.

(ii) In the thermal balance (equation (5)) the losses due to sublimation are not taken into account. The thermal balance calculations for the dust particles made by taking this factor into consideration (Shestakova and Tambovtseva, 1995) showed that its influence on the thermal balance at $T < 1600$ K (silicate) and at $T < 2200$ K (graphite) is negligible. This condition is always valid for graphite at distances $R > 4r_\odot$ and for silicate for $R \geqslant 9r_\odot$, where the surface temperature is about 1370 K. For ice, we restricted ourselves to the regions $R > 3$ AU, where the sublimation process is negligibly small (Shulman, 1987). Thus, we use the black-body approximation to estimate the surface temperature of the solids of any material.

(iii) The loss due to heat conduction is neglected. This means that $\sigma T_s^4 > \kappa(T_s)\, \mathrm{d}T/\mathrm{d}x|_{x=r}$. Such an approximation is quite valid for non-icy solids at high temperatures as well as for small icy solids ($r < 100$ m). However, even for larger icy solids, T_s does not decrease significantly because of the losses due to heating inside the solid (Kürt, 1984). The thermal hysteresis, which appears as a consequence of the heat conductivity to the core when the solid moves towards and away from the perihelion, does not exceed the daily variations in the temperature T_s. The decrease in T_s due to the appearance of the coma can also be neglected at distances $R > 3$ AU.

Thus, smoothing all surface temperature variations and assuming that the surface is in radiative equilibrium with the solar radiation and is isothermal, we obtain the surface boundary condition in the form

$$T_s(t) = \frac{T_{\mathrm{eff}}}{(2R/r_\odot)^{1/2}},$$

where $[(1-A)/\varepsilon]^{1/4} \approx 1$, since consideration of these parameters does not have any significance.

The main procedure for obtaining an analytical HDE solution is the representation of $T_s(t)$ as a direct function of the time t. This becomes possible for parabolic orbits with a perihelion $q \approx 0$. In common cases the time of passage of the solids from the distance R to the perihelion for the parabolic orbits has the form

$$\tau(R) = \left(\frac{2}{GM_\odot}\right)^{1/2}\left(\frac{(R-q)^{3/2}}{3} + q(R-q)^{1/2}\right).$$

Thus, at $q = 0$ it follows that $\tau(R) = (2/GM_\odot)^{1/2}R^{3/2}/3$, where G is the gravitational constant and $M_\odot$ is the mass of the Sun. As a result we obtain the boundary condition required:

$$T_s(t) = \frac{T_0}{(1 - t/\tau_0)^{1/3}},$$

where $T_0 = T_{\mathrm{eff}}/2R_0/r_\odot)^{1/2}$ is the temperature of the solid at the initial distance R_0, τ_0 is the time that the solid takes to fall on to the Sun from this distance and $t = \tau_0 - \tau(R)$ is the current time.

The HDE solution permits us to derive the temperature distribution inside the solid at any distance from the Sun for any material with known thermal parameters.

5.2 Basic formulae for the thermal stresses

When heating or cooling a solid, radial stresses σ_{rr} and tangential stresses $\sigma_{\phi\phi}$ appear. Expressions for these were obtained by Boley and Weiner (1960). It is easy to distinguish from these stresses those functions that have a temperature dimension. An analysis of the thermal stresses originating in the solid bodies will be significantly simplified if we use temperature functions instead of the thermal stresses themselves. The former depend on only the body's geometry and temperature distribution.

Using these temperature functions as analogous to the thermal stresses, we can easily obtain the stresses with the help of the simple link

$$\sigma_{\phi\phi}(x) = \frac{E\alpha}{1-\mu} T_{\phi\phi}(x), \qquad \sigma_{rr}(x) = \frac{E\sigma}{1-\mu} T_{rr}(x), \tag{6}$$

where the tangential stresses $\sigma_{\phi\phi}(x)$ are characterized by the function $T_{\phi\phi}(x)$, and the radial stresses σ_{rr} by the function $T_{rr}(x)$. Here we used the parameters characterizing the elastic and thermal features of the material: Young's modulus E, Poisson's ratio μ and the linear expansion coefficient α.

The temperature functions obtained from the solution of Boley and Weiner (1960) have the forms

$$T_{\phi\phi}(x) = \frac{2}{r^3}\int_0^r T(y)y^2\,\mathrm{d}y + \frac{1}{x^3}\int_0^x T(y)y^2\,\mathrm{d}y - T(x), \tag{7}$$

$$T_{rr}(x) = \frac{2}{r^3}\int_0^r T(y)y^2\,\mathrm{d}y - \frac{2}{x^3}\int_0^x T(y)y^2\,\mathrm{d}y, \tag{8}$$

Here $T(y)$ is the radial temperature profile obtained after solving HDE.

Thus, the radial stresses σ_{rr} and tangential stresses $\sigma_{\phi\phi}$, which originate when the solid bodies are heated or cooled, are determined by the corresponding temperature functions T_{rr} and $T_{\phi\phi}$ and by the elastic parameters of the material.

In the case when $\sigma_{\phi\phi}$ or σ_{rr} is negative, the material undergoes compression; when they are positive, the material is subject to tension (Campbell, 1956). The same is valid for the temperature functions.

The temperature profile according to the analytical solution of the HDE by Shestakova and Tambovtseva (1997–1998, equation (A8)) can be found from

$$T(x,t) = \frac{T_0}{(1-t/T_0)^{1/3}} - \frac{2T_0 r\tau_c}{3\pi x\tau_0}\sum_{n=1}^{\infty}\frac{(-1)^{n-1}\sin(\pi nx/r)}{n^3}\int_0^b \frac{\exp(-y)\,\mathrm{d}y}{(1-t/\tau_0+\tau_c t/\tau_0 n^2)^{4/3}} \tag{9}$$

or, after integrating by parts,

$$\begin{aligned} T(x,t) = T_s(t) - \frac{\pi^2 T_0\tau_c[1-(x/r)^2]}{18\tau_0(1-t/\tau_0)^{4/3}} + \frac{2T_0 r\tau_c}{3\pi x\tau_0}\sum_{n=1}^{\infty}\frac{(-1)^{n-1}\sin(\pi nx/r)}{n^3}\exp(-b) \\ + \frac{8T_0 r}{9\pi x}\left(\frac{\tau_c}{\tau_0}\right)^2\sum_{n=1}^{\infty}\frac{(-1)^{n-1}\sin(\pi nx/r)}{n^5}\int_0^b \frac{\exp(-y)\,\mathrm{d}y}{(1-t/\tau_0+\tau_c y/\tau_0 n^2)^{7/3}}. \end{aligned} \tag{10}$$

This means that, for small bodies for which $\tau_c/\tau_0 \ll 1$, the temperature profile is given by a simple expression since the influence of the series is negligible. Thus, the difference between the temperatures of the surface of the body and of its centre is, to a first approximation,

$$\Delta T = \frac{\pi^2 T_0 \tau_c}{18\tau_0(1 - t/\tau_0)^{4/3}} = \frac{\pi^2 T_s(t)\tau_c}{18\tau(R)} = \frac{\pi^2 T_{\text{eff}}(GM_\odot r_\odot)^{1/2}\tau_c}{12R^2}. \tag{11}$$

From here, one may see that for a solid falling on to the Sun the difference between the temperature of its center and of the surface increases rather quickly with decreasing distance to the Sun (T is proportional to $1/R^2$), while the temperature of the solid's surface increases more
slowly ($T_s(t)$ is proportional to $1/R^{1/2}$). Equation (11) fails when $\tau_c/\tau(R) \geqslant 1$, that is when the cooling or heating time is greater than the time that the solid takes to fall on to the Sun from a given distance R.

Using equation (9) for the temperature profile we obtain the solution for the temperature functions (equations (7) and (8)). For this, we denote the first term in equation (9), which is equal to the temperature at the surface, as T_s and the integral in the same expression as $J(n)$. Then we introduce the following definitions:

$$A = \frac{2}{r^3}\int_0^r T(y)y^2\,\mathrm{d}y, \qquad B(x) = \frac{1}{x^3}\int_0^x T(y)y^2\,\mathrm{d}y. \tag{12}$$

After substituting $T(y)$ from equation (9) and integrating, we obtain

$$A = \frac{2T_s}{3} - \frac{4T_0\tau_c}{3\pi^2\tau_0}\sum_{n=1}^{\infty}\frac{J(n)}{n^4},$$

$$B(x) = \frac{T_s}{3} - \frac{2T_0 r^2\tau_c}{3\pi^2 x^2\tau_0}\left(\frac{r}{\pi x}\sum_{n=1}^{\infty}\frac{(-1)^{n-1}J(n)\sin(\pi nx/r)}{n^5} - \sum_{n=1}^{\infty}\frac{(-1)^{n-1}J(n)\cos(\pi nx/r)}{n^4}\right). \tag{13}$$

As a result the expressions for the temperature functions (equations (7) and (8)) transform into

$$T_{\phi\phi}(x) = A + B(x) - T(x), \qquad T_{rr}(x) = A - 2B(x), \tag{14}$$

whose numerical solution, together with $T(x)$, is obtained comparatively easily since most of the time required is taken by the calculation of the integral $J(n)$. Note, however, that this integral is the same for all three function: $T_{\phi\phi}(x)$, $T_{rr}(x)$ and the temperature $T(x)$ itself.

5.3 Solids in the F corona

At a distance of $9r_\odot$ from the Sun the temperature of the bodies on the surface reaches the melting point of iron olivine and iron proxyene (1370 K according to Krinov (1995)). Since these minerals are the basis of the chondrite material, all products of the fragmentation and the dust disintegrate quickly at this distance, forming a refractory dust, mainly consisting of magnesium olivine and pyroxene. Non-refractory dust sublimates into the gas phase.

The surface destruction of the large bodies increases when the material starts to melt. Even very small radial stresses under the surface of the large solids become sufficient to throw off

the outer layer. Because of the melting process, the surface temperature becomes stable and a quick internal heating of the solid begins, with a rapid increase in the stresses. Solids with $r > 10$ m, which have stresses close to critical values, will disintegrate near the melting boundary. Only solids of essentially larger sizes can penetrate significant distances inside melting boundary without catastrophic destruction, but with significant surface losses.

Thus, if a meteor stream moving along an elongated orbit moves into the circumsolar region, one may expect a rapid sublimation of small solids, the destruction of the surface of large solids and the catastrophic destruction of solids with intermediate sizes which form dust and gas streams at a distance of less than $9r_\odot$.

Increases in dust thermal emission at this distance as well as at $4r_\odot$ have been detected during the total solar eclipses by MacQueen (1968) at $\lambda = 2.2$ μm. Keeler and Lidenberg (1981) found an emission at $9r_\odot$ through observations in the range $\lambda = 0.7$–2.2 μm. It should be noted that during the solar eclipse in 1980, Zirker (1984) did not detect such an increase at $4r_\odot$.

The melting point of the more refractory magnesium olivine, 2160 K (Krinov, 1995), is reached at a distance of about $4r_\odot$. By observing the infrared increase at this distance Peterson (1971) determined the temperature as 2160 ±200 K. It is interesting to note that this value coincides with the melting point of the magnesium olivine. An estimation of the sizes of particles responsible for the formation of the thermal emission increase near $4r_\odot$ made by Maihara *et al.* (1985) showed that the radii of these particles had to be very large; they exceed 100 μm. These results contradict the observations of Léna *et al.* (1974) and Mankin *et al.* (1974) in the mid-infrared region at $\lambda \approx 10$ μm, who concluded that many small submicron particles have to exist in the F corona.

In our opinion, this contradiction disappears completely if the nature of the local infrared increases is not connected with the common background scattering and the thermal emission of the dust particle having a zodiacal nature. This excess could be caused by the thermal emission of the large dust particles appearing due to the splitting and/or fragmentation of the solids. This result agrees with that of Hodapp *et al.* (1992) who concluded that the increase in the infrared emission could be attributed to the transient dust injected into circumsolar space by Sun-grazing comets.

5.4 Icy solids

Observations of comets in the Solar System show that there is a mineral dust on their surface which causes the low albedo of the comet nuclei (Shulman, 1987). This dust serves as a screen for the ice nucleus. Close to the Sun, the formation of the coma also significantly changes the thermal regime of the surface of the nucleus.

Nevertheless, at larger distances from the Sun, one could consider the influence of all these factors for the problem of interest to be negligible. When a coma develops, heating of the ice surface almost stops (Shulman, 1987). On further approaching the Sun the thermal stresses accumulated at that moment either retain their values or increase slightly.

The scenario of disruption of the icy body is qualitatively similar to that mentioned above but has its own peculiar features. Because the low strength of the icy material, surface destructions occur in the deeper layer and become manifest at great distances from the Sun (more than 40 AU for bodies with $r \geqslant 1$ km). It can be seen (Figure 7) that in the centre of icy bodies with radii greater than 1 km the temperature is equal to the black-body value assumed at the initial distance. Small solids (30 m and smaller) are almost isothermal and the temperatures in their interior are very close to the surface temperature (dotted curve). The 'analytical' results are shown as dashed curves for a radius of 1 km or greater the results coincide.

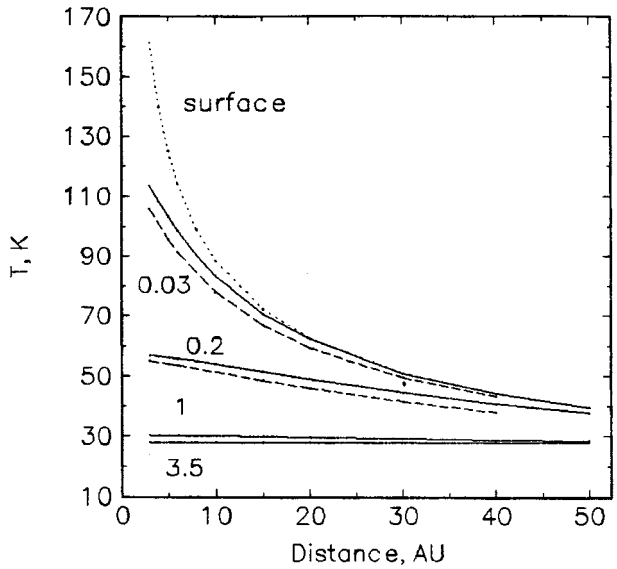

FIGURE 7 The behaviour of the temperature in the centres of icy solids on approaching the Sun. The numbers indicate the radii of the solids in kilometres. The dotted curve shows the change in the temperature at the surface. The dashed line is the analytical result, the solid line is the numerical one.

It can be seen from Table 1 that the disintegration of icy bodies with $r \approx 1$ km could begin first of all at a distance of 40 AU. Bodies of both larger and smaller sizes may experience catastrophic disruption nearer the Sun. Table 1 shows that splitting of the cometary nuclei depends on the initial radius of these nuclei and can occur at very different places on the orbit when moving towards the Sun. Finally, the bodies with $r > 6$ km do not reach the tensile strength.

If the bodies start from the Kuiper belt (30 AU), because of the higher initial temperature in their centres, the large icy bodies become stable to thermal destruction (Table 2). The boundary of stability is shifted towards the lower radius. Thus, bodies with $r \geqslant 2.2$ km do not reach the critical internal stresses at distances $R > 3$ AU. It should be noted that for bodies with $r < 220$ m the choice of the initial distance is not necessary.

A body such as the comet Shoemaker–Levy 9 which, before disintegration, had an initial radius $r = 0.9$ km and a density of $0.6\,\mathrm{g\,cm^{-3}}$ (Solem, 1995) would, according to our scenario, be destroyed owing to thermal stresses at a great distance from the Sun and

TABLE 1. The critical distances for the thermal destruction of icy bodies (starting from the Oort cloud ($T_0 = 28$ K)).

Radius (km)	Distance (AU)
6	—
5.1	5
3.5	10
1.0	40
0.2	25
0.03	10
0.01	3

TABLE 2. The critical distances for the thermal destruction of icy bodies starting from the Kuiper belt ($T_0 = 51$ K)).

Radius (km)	Distance (AU)
2.2	—
1.5	5
0.7	10
0.2	18
0.03	10
0.01	3

would approach Jupiter's orbit already in the form of a chain of fragments, elongated along the orbit. Thus, only large interstellar guests with $r > 6$ km could penetrate the Solar System without destruction.

A comparison of the thermal stresses with those caused by the tidal forces shows that the effect of the latter on icy bodies is weaker by four to five orders of magnitude even in the most favourable cases and we may conclude that the thermal stresses affect the evolution of the cometary nuclei much more effectively than do the tidal forces.

6 CONCLUSION

(i) A detailed analysis of the thermal stresses at the surface and in the interior of solids approaching the Sun with parabolic orbits has revealed a similarity in the behaviour of solids of all the material considered.
   (a) A range of distances from the Sun and a range of body sizes exist for which the internal thermal stresses exceed the material strength known from physical experiments.
   (b) For such bodies the crucial stresses are reached earlier than the time at which initiation of the surface melting process begins.
   (c) There are solid sizes for which the distance when the thermal stresses exceed the material strength is far from the Sun (e.g. comets with radii equal to 1 km at a distance of about 40 AU); larger and smaller solid bodies will experience the same internal stresses substantially later, that is much nearer to the Sun.
   (d) By contrast, the surface (compressive) stresses increase with increasing radius of the body. Therefore, the destruction of the surface of large bodies (accompanying coma formation in icy solids) will occur substantially earlier, at remote distances from the Sun.

(ii) So, the mechanism of the thermal disintegration may play a crucial role in cometary splitting. It should be noted that for the actual stretching of fragments along the orbit forces, stresses other than thermal stresses are requested. Self-gravity could hold the fragments together for some time, but such mechanisms as tidal forces, rapid rotation, and the presence of irregular objects or volatiles in the solids may overcome self-gravity and elongate the fragments along the orbit.

(iii) Our results allow us to explain the episodic appearance of increases in the thermal infrared emission in the F corona at $4r_\odot$ and $9r_\odot$ if one accepts that the basis of the silicate material is olivine and pyroxene. These local maxima may be caused by the dust particles appearing owing to the thermal destruction of the solids.

(iv) During the total solar eclipse of February 26, 1998, the spacious area of emission in the H and K lines of Ca II at distances from $3.5r_{\odot}$ to $18r_{\odot}$ was discovered by Gulyaev and Shcheglov (1999a,b) to the west of the Sun. Numerical estimations have shown that the main reason for ion acceleration is the radiation pressure.

(v) The presence of cold gas which is not typical for a solar corona, containing short-lived Ca ions, may be explained by penetration in the solar corona of comet-like matter which, after thermal destruction and full or partial evaporation, transforms into gas.

Our investigations of processes of transition of dust and small bodies into gas in the circumsolar region (similar to the process taking place near β-Pictoris) is unique and further development of this work is required.

References

Aimanov, A. K., Aimanova, G. K., and Shestakova, L. I. (1995) *Astron. Lett.* **21**, 196.
Alfvén, G., and Feltkhammar, K.-G. (1967) *Space Electrodynamics*, Mir, Moscow (in Russian).
Allen, C. W. (1963) *Astrophysical Quantities*, 2nd edition, Athlone, London.
Aumann, H. H., Gillett, F. C., Beichman, C. A., de Jong, T., Houck, T. J. R., Low, F. J., Neugebauer, G., Walker, R. G., and Wesselius, P. R. (1984) *Astrophys. J.* **278**, L23.
Bailey, M. E. (1996) *Earth, Moon, Planets* **72**, 57.
Benz, W., and Asphaug, E. (1994) *Lunar Planet. Sci.* **25**, 101.
Beust, H., Lagrange-Henri, A. M., Vidal-Madjar, A., and Ferlet, R. (1989) *Astron. Astrophys.* **223**, 304.
Beust, H., Lagrange-Henri, A. M., Vidal-Madjar, A., and Ferlet, R. (1990) *Astron. Astrophys.* **236**, 202.
Beust, H., and Morbidelli, A. (1996) *Icarus* **120**, 358.
Boley, B. A., and Weiner, J. H. (1960) *Theory of Thermal Stress*, Wiley, New York, p. 302.
Campbell, I. E. (ed.) (1956) *High-Temperature Technology*, Wiley, New York.
Chen, J., and Jewitt, D. (1994) *Icarus* **108**, 265.
Clube, S. V. M., and Napier, W. M. (1987) *Mon. Not. R. Astron. Soc.* **225**, 55P.
Dobrovolskis, A. R. (1990) *Icarus* **88**, 24.
Grinin, V. P., Natta, A., and Tambovtseva, L. V. (1996) *Astron. Astrophys.* **313**, 857.
Gurtovenko, E. A. (1971) *Solar Phys.* **16**, 413.
Gulyaev, R. A., and Shcheglov, P. V. (1999a) *Dokl. Akad. Nauk (Russia)* **366**, 199.
Gulyaev, R. A., and Shcheglov, P. V. (1999b) *Izv. Akad. Nauk (Russia), Ser. Fiz.* **63**, 2186.
Gulyaev, R. A., and Shcheglov, P. V. (2001) *Usp. Phys. Nauk (Russia)* **171**, 217.
Hodapp, K.-W., MacQueen, R. M., and Hall, D. N. B. (1992) *Nature* **355**, 707.
Keeler, C. F., and Liedenberg, D. (1981) *Los Alamos Science, LANL* **2**, 4.
Krinov, E. A. (1995) *Osnovi Meteoritiki*, Nauka, Moscow, p. 392.
Koutschmy, S. (1998) Private communication to R. A. Gulyaev.
Kürt, E. (1984) *Icarus* **60**, 512.
Lagrange-Henri, A.-M., Plazy, F., Beust, H., Mouillet, D., Deleuil, M., Ferlet, R., Spyromilio, J., Vidal-Madjar, A., Tobin, W., Hearnshaw, J. B., Clark, M., and Tomas, K. W. (1996) *Astron. Astrophys.* **310**, 547.
Lamy, P. L. (1974) *Astron. Astrophys.* **35**, 197.
Lamy, P. L., Kuhn, J. R., Lin, H., Koutchmy, S., and Smartt, R. N. (1992) *Science* **257**, 1377.
La Violette, P. A. (1987) *Mon. Not. R. Astron. Soc.* **224**, 945.
Léna, P., Viala, Y., Hall, D., and Soufflot, A. (1974) *Astron. Astrophys.* **37**, 81.
MacQueen, R. M. (1968) *Astrophys. J.* **154**, 1059.
Maihara, T., Mizutani, K., Hiromoto, N., Takami, H. and Hasegawa, H. (1985) In: R. N. Giese and P. L. Lamy (eds), *Properties and Interactions of Interplanetary Dust*, Reidel, Dordrecht, p. 55.
Mankin, W. G., MacQueen, R. M., and Lee, R. H. (1974) *Astron. Astrophys.* **31**, 17.
Mann, I., and MacQueen, R. M. (1993) *Astron. Astrophys.* **275**, 293.
Mann, I., Okamoto, H., Mukai, T., Kimura, H., and Kitada, Y. (1994) *Astron. Astrophys.* **291**, 1011.
Minnaert, M., Mulders, G. F. W., and Houtgast, J. (1940) *Photometric Atlas of Solar Spectrum*, Sonnenborgh, Utrecht.
Mukai, T., and Yamamoto, T. (1979) *Publ. Astron. Soc. Japan* **31**, 585.
Peterson, A. W. (1967) *Astrophys. J.* **148**, L37.
Peterson, A. W. (1971) *Bull. Am. Astron. Soc.* **3**, 500.
Pittish, E. M., and Rickman, H. (1994) *Astron. Astrophys.* **281**, 579.
Sekanina, Z. (1982) In: L. L. Wilkening (ed.), *Comets*, University of Arizona Press, Tucson, Arizona, p. 251.
Sekanina, Z. (1997) *Astron. Astrophys.* **318**, L5.
Shcheglov, P. V., Shestakova, L. I., and Aimanov, A. K. (1987) *Astron. Astrophys.* **173**, 383.
Shestakova, L. I. (1987) *Astron. Astrophys.* **175**, 289.

Shestakova, L. I. (1990) *Soviet Astron. Lett.* **16**, 550.
Shestakova, L. I., and Tambovtseva, L. V. (1995) *Astron. Astrophys. Trans.* **8**, 59.
Shestakova, L. I., and Tambovtseva, L. V. (1997–1998) *Earth, Moon, Planets* **76**, 19.
Shulman, L. M. (1987) *Yadra Komet*, Nauka, Moscow, p. 232.
Smith, B. A., and Terrile, R. J. (1984) *Science* **226**, 1421.
Solem, J. C. (1995) *Astron. Astrophys.* **302**, 596.
Steel, D. I. (1996) *Earth, Moon, Planets* **72**, 279.
Tambovtseva, L. V., and Shestakova, L. I. (1999) *Planet. Space Sci.* **47**, 319.
Tauber, F., and Kürt, E. (1987) *Icarus* **69**, 83.
Vidal-Madjar, A., Lagrange-Henri, A.-M., Feldman, P. D., Beust, H., Lissauer, J. J., Deleuil, M., Ferlet, R., Gry, C., Holbs, L. M., McGrath, M. A., McPhate, J. B., and Moos, H. W. (1994) *Astron. Astrophys.* **290**, 245.
Zirker, J. B. (1984) *Total Eclipse of the Sun*, Van Nostrand Reinhold, New York, p. 210.